Topology-insensitive axion mass in magnetic topological insulators

Koji Ishiwata

Institute for Theoretical Physics, Kanazawa University, Kanazawa 920-1192, Japan

We study the axion in three-dimensional topological insulators with magnetic impurities under finite temperature. We find a stable antiferromagnetic ground state and ferromagnetic metastable state. In both magnetic states, the mass of the axion is found to be up to eV scale and it approaches zero near the phase boundary of the magnetic state. This result applies to both normal and topological insulator phases, i.e., the axion mass is insensitive to the topological states and it will have a direct impact on the targeted mass range of particle axion dark matter in future experiments.

I. INTRODUCTION

The axion has drawn attention in interdisciplinary fields of particle physics, cosmology, and condensed matter physics. In condensed matter physics, a dynamical axion is predicted in the magnetic topological insulators (TIs) [1]. It is a quasiparticle that couples to the electromagnetic fields, which leads to an instability of the electromagnetic fields. It is predicted that the instability causes the total reflection of the incident light [1] or the conversion of the external electric field to magnetic field [2]. On top of that, it was proposed in Refs. [3–5] that the axion in the magnetic TIs can be a possible excitation signal in the detection of the *particle* axion, which is a good candidate for dark matter of the universe. On the other hand, a static axion or constant axion is known as the magnetoelectric effect [6–11]. To understand the properties of both the dynamical and static axions, magnetism plays a crucial role.

In Refs. [12–14], the dynamical axion in the antiferromagnetic (AFM) TIs is described from the partition function given by the path integral. As a result, the mass of the dynamical axion in the AFM TIs is estimated to be about a meV. This mass range corresponds to the projected mass range of the *particle* axion proposed by the authors of Ref. [3]. On the other hand, the author of Ref. [15] revisited the axion mass in the Hubbard model and reformulated the action of the axion field using the Hubbard-Stratonovich transformation. In the formula, the effective potential for the axion field is derived in the topological and normal insulators under the AFM and paramagnetic states. Consequently, both the dynamical and static axions are described consistently and the axion mass is found to be less than $\mathcal{O}(\text{eV})$. Furthermore, it can be suppressed near the phase boundary between the AFM and paramagnetic states. Since the axion mass in materials directly corresponds to the mass range of the *particle* axion in the proposal of any future axion detection experiment [3], the evaluation of the axion mass in materials is crucial.

In recent years, magnetically doped bismuth selenide or bismuth telluride has caught lots of attention. For example, both the AFM and ferromagnetic (FM) states are predicted in

$MnBi_2Te_4$ [16–20] or $Mn_2Bi_2Te_5$ [21] by the first-principles calculations. Regarding $Mn_2Bi_2Te_5$, a rich magnetic topological state in addition to the AFM/FM states are predicted [21].[1] Since such materials are probable candidates for the detection of the particle axion, it is important to find how to describe the axion in a variety of magnetic states.

In this work, we formulate the axion in the TIs with magnetic dopants under finite temperature. For this purpose, we consider the three-dimensional (3D) effective TIs model with the interaction term of electrons with magnetic impurities. In this study we do not specify the explicit material. The grand potential is calculated from the path integral under finite temperature, and consequently, the effective potential for the order parameter of the AFM and FM are derived. Around the stationary points of the effective potential, the mass of the dynamical axion is formulated. We will see that the typical mass scale of the axion in the magnetic insulators is eV and it can be suppressed near the phase boundary, depending on temperature. This feature is insensitive to the topological states of insulators. As a check, we will also see that the curvatures with respect to the order parameters of the AMF and FM phases correspond to the Van Vleck-type spin susceptibility, which is calculated in the linear perturbation theory, for a band insulator. The result implies that the mass range of the *particle* axion which is projected to be probed [3] is around eV scale and it depends on the magnetic state of the insulators. The temperature dependence of the axion mass might be used to search for low-mass regions.

This paper is organized as follows. In the next section, we give the Hamiltonian of the model and define the observables including the order parameters. In Sec. III the effective potential for the order parameters is derived from the grand potential, which gives rise to the phase diagram of magnetism

---

[1]The dynamical axion was studied in Ref. [22], and recently the authors of Ref. [23] reported that $Mn_2Bi_2Te_5$ is synthesized and its experimental aspects are studied.

in Sec. IV. Finally, the axion mass is derived in Sec. V. The conclusion is given in Sec. VI.

II. MODEL

We consider a effective model for 3D topological insulators (TIs). The basic Hamiltonian is [1,24][2]

$$H^{\text{TI}} = \sum_{k} c_{k}^{\dagger} \mathcal{H}_{k}^{\text{TI}} c_{k}, \tag{2.1}$$

$$\mathcal{H}_{k}^{\text{TI}} = (\epsilon_{0} - \mu)\mathbf{1} + \sum_{a=1}^{4} d^{a} \Gamma^{a}, \tag{2.2}$$

where $c_{k}^{\dagger}$ and c_{k} are the creation and annihilation operators of electrons in the wave-number space and μ is the chemical potential, k is the wave number, and Γ^{a} are the Gamma matrices defined in Eq. (A1) of Appendix A. ϵ_{0} is a constant and d^{a} is parameterized as

$$(d^{1}, d^{2}, d^{3}, d^{4}) = (A_{2} \sin k_{x} \ell_{x}, A_{2} \sin k_{y} \ell_{y}, A_{1} \sin k_{z} \ell_{z}, \mathcal{M}), \tag{2.3}$$

where $\mathcal{M} = M_{0} - 2B_{1} - 4B_{2} + 2B_{1} \cos k_{z} \ell_{z} + 2B_{2} (\cos k_{x} \ell_{x} + \cos k_{y} \ell_{y})$. $M_{0} < 0$ and $M_{0} > 0$ correspond to topological and normal insulators, respectively. We consider a cubic lattice in the later analysis, i.e., $\ell_{x} = \ell_{y} = \ell_{z} \equiv \ell$, for simplicity. The Hamiltonian has the time-reversal invariance, which is one of the features of the TIs, and it describes the $Bi_{2}Se_{3}$ family of materials, including $Bi_{2}Te_{3}$ and $Sb_{2}Te_{3}$ [25]. In the present study, we additionally assume magnetic dopants, such as Fe, Cr, or Mn, in the material and introduce the on-site interaction term between the impurity and electron [26]

$$H_{J} = \sum_{I}^{N_{s}} \left[J^{A} S^{A}(x_{I}) \cdot s_{I}^{A} + J^{B} S^{B}(x_{I}) \cdot s_{I}^{B} \right], \tag{2.4}$$

where S^{A} (s_{I}^{A}) and S^{B} (s_{I}^{B}) are the local spins of the impurities (spins of electron) at cite I of the sublattices A and B, respectively. J^{A} and J^{B} are the exchange coupling constants and N_{s} is the number of the impurities. In the following discussion, we consider the magnetism in the z direction. Then the spins of electron are written as

$$s_{zI}^{A} = \tfrac{1}{2} c_{I}^{\dagger} (\Gamma^{12} + \Gamma^{5}) c_{I}, \tag{2.5}$$

$$s_{zI}^{B} = \tfrac{1}{2} c_{I}^{\dagger} (\Gamma^{12} - \Gamma^{5}) c_{I}, \tag{2.6}$$

where c_{I} is the wave function of the electron at cite I in the lattice space and Γ^{12} and Γ^{5} are given in Appendix A. The similar model, but only with a term proportional to Γ^{12} is considered in Refs. [27–29] in a different context. In Ref. [29], the same terms as both Γ^{12} and Γ^{5} are considered. In the literature, Cr and Mn are doped on the top and the bottom halves of the TI films in superlattice and the exchange couplings with Cr and Mn are taken to be opposite each other. Then the mass of the dynamical axion is estimated to be meV. We will get a different result in Sec. V.

We apply the mean-field approximation (MFA) to H_{J}. In the MFA, H_{J} becomes

$$
\begin{aligned}
H_{J} \approx \sum_{I}^{N_{s}} & \left[J^{A} \langle S_{z}^{A} \rangle s_{zI}^{A} + J^{B} \langle S_{z}^{B} \rangle s_{zI}^{B} \right. \\
& + J^{A} S_{z}^{A}(x_{I}) \langle s_{z}^{A} \rangle + J^{B} S_{z}^{B}(x_{I}) \langle s_{z}^{B} \rangle \big] \\
& - N_{s} \big(J^{A} \langle S_{z}^{A} \rangle \langle s_{z}^{A} \rangle + J^{B} \langle S_{z}^{B} \rangle \langle s_{z}^{B} \rangle \big).
\end{aligned}
\tag{2.7}
$$

Introducing

$$M^{A} = x \langle S_{z}^{A} \rangle, \qquad M^{B} = x \langle S_{z}^{B} \rangle, \tag{2.8}$$

$$m^{A} = \langle s_{z}^{A} \rangle, \qquad m^{B} = \langle s_{z}^{B} \rangle, \tag{2.9}$$

where $x = N_{s}/N$ and N is the number of cite, we get

$$
\begin{aligned}
H_{J} \approx \sum_{i}^{N} & \left[J^{A} M^{A} s_{zi}^{A} + J^{B} M^{B} s_{zi}^{B} \right] \\
& + \sum_{I}^{N_{s}} \left[J^{A} m^{A} S_{z}^{A}(x_{I}) + J^{B} m^{B} S_{z}^{B}(x_{I}) \right] \\
& - N(J^{A} M^{A} m^{A} + J^{B} M^{B} m^{B}).
\end{aligned}
\tag{2.10}
$$

As a result, the total Hamiltonian is linearized as[3]

$$H^{\text{TI}} + H_{J} \approx H_{e} + H_{S} + H_{R}, \tag{2.11}$$

where H_{e} and H_{S} are the Hamiltonians of the electrons and the local spin defined by

$$H_{e} = H^{\text{TI}} + \sum_{i}^{N} \left[J^{A} M^{A} s_{zi}^{A} + J^{B} M^{B} s_{zi}^{B} \right], \tag{2.12}$$

$$H_{S} = \sum_{I}^{N_{s}} \left[J^{A} m^{A} S_{z}^{A}(x_{I}) + J^{B} m^{B} S_{z}^{B}(x_{I}) \right], \tag{2.13}$$

$$H_{R} = -N(J^{A} M^{A} m^{A} + J^{B} M^{B} m^{B}). \tag{2.14}$$

For later analysis, it is convenient to write down the Hamiltonian by using the following variables:

$$m_{t} = m^{A} + m^{B}, \tag{2.15}$$

$$m_{r} = m^{A} - m^{B}, \tag{2.16}$$

$$M_{f} = \tfrac{1}{2}(J^{A} M^{A} + J^{B} M^{B}), \tag{2.17}$$

$$M_{5} = \tfrac{1}{2}(J^{A} M^{A} - J^{B} M^{B}). \tag{2.18}$$

M_{f} and M_{5} plays the order parameters of the FM and AFM, respectively. In terms of M_{f} and M_{5} the Hamiltonian of the electrons is given by

$$H_{e} = \sum_{k} c_{k}^{\dagger} \mathcal{H}_{ek} c_{k}, \tag{2.19}$$

---

[2]We change the notation of Hamiltonian from one in Ref. [15].

[3]Although M^{A}, M^{B}, m^{A}, and m^{B} themselves should be interpreted as the mean-field values (or vacuum expectation values), we take them as spurious fields to give the effective potential. See the later discussion.

where[4]

$$\mathcal{H}_{e\boldsymbol{k}} = \mathcal{H}_{\boldsymbol{k}}^{\mathrm{TI}} + \mathcal{H}_{\boldsymbol{k}}^{m}, \tag{2.20}$$

$$\mathcal{H}_{\boldsymbol{k}}^{m} = M_f \Gamma^{12} + M_5 \Gamma^5. \tag{2.21}$$

We note that the two terms proportional to Γ^{12} and Γ^5 appear in the Hamiltonian for the electrons. Those terms describe the magnetism of the materials and they are consistent with the symmetry of the crystal structure of the materials, such as Bi_2Se_3 and Bi_2Te_3 [25]. Diagonalizing $\mathcal{H}_{e\boldsymbol{k}}$ gives four energy bands. They are given by $E_{j\boldsymbol{k}} = \epsilon_0 - \mu \pm e_{j\boldsymbol{k}}$ ($j = 1, 2$), where

$$e_{1\boldsymbol{k}} = \sqrt{d_0^2 + M_f^2 + M_5^2 + 2M_f \sqrt{d_s^2 + M_5^2}}, \tag{2.22}$$

$$e_{2\boldsymbol{k}} = \sqrt{d_0^2 + M_f^2 + M_5^2 - 2M_f \sqrt{d_s^2 + M_5^2}}, \tag{2.23}$$

where $d_0 \equiv \sqrt{\sum_{a=1}^{4} d^a d^a}$ and $d_s \equiv \sqrt{(d^3)^2 + (d^4)^2}$.

In the following discussion, we consider the half-filling case since we are interested in the insulator in the bulk. In addition we assume that the temperature is sufficiently smaller than the energy scale of the electron. This is a good approximation since we consider temperature up to $\mathcal{O}(10^2\,\mathrm{K})$. Then the chemical potential should be chosen as $\mu \simeq \epsilon_0$, and the relevant energy bands in the following discussion are going to be $-e_{1\boldsymbol{k}}$ and $-e_{2\boldsymbol{k}}$.

III. EFFECTIVE POTENTIAL FROM THE GRAND POTENTIAL

While the mean-field values for each variable can be derived from the Hamiltonian, the grand potential is useful to derive the effective action for the order parameters M_f and M_5. The grand potential is given by[5]

$$\Omega = -\beta^{-1} \ln Z, \tag{3.1}$$

where $\beta = 1/T$ is the inverse temperature and Z is the partition function given by

$$Z = \int \mathcal{D}c^\dagger \mathcal{D}c \mathcal{D}M \, e^{-S_E}. \tag{3.2}$$

Here c is the wave function of the electrons, M represents S_z^A and S_z^B, and S_E is the action of the system in the Euclidean space.[6] The Hamiltonian of the electrons and local spins are linearized under the MFA, as seen in the previous section. Then the Euclidean action is given by $S_E = S_e + S_S + S_R$ where

$$S_e = \int_0^\beta d\tau \sum_i^N c_i^\dagger [\partial_\tau + \mathcal{H}_e] c_i, \tag{3.3}$$

---

[4]M_5 corresponds to ϕ in Ref. [15].

[5]Since we consider the half-filling case, the grand potential corresponds to the Helmholtz free energy.

[6]In the derivation of the kinetic term of the dynamical axion, we promote M_5 to a dynamical field. See the later discussion and Appendix D.

$$S_S = \int_0^\beta d\tau H_S, \tag{3.4}$$

$$S_R = \int_0^\beta d\tau H_R = \beta H_R. \tag{3.5}$$

Consequently, the grand potential is obtained as

$$\Omega = \Omega_e + \Omega_S + H_R, \tag{3.6}$$

where Ω_e is the grand potential for the electrons and Ω_S is the one for the local spins given by

$$\Omega_S = -\beta^{-1} N_s \left[\ln \frac{\sinh(S + 1/2)\beta J^A m^A}{\sinh \beta J^A m^A / 2} + (A \to B) \right]. \tag{3.7}$$

Here S is the absolute value of the local spin. Ω_e, on the other hand, is computed as

$$\Omega_e = -\beta^{-1} \ln e^{-\mathcal{S}_e}, \tag{3.8}$$

$$\mathcal{S}_e = -\ln \det[\partial_\tau + \mathcal{H}_e]. \tag{3.9}$$

Here the determinant is obtained by

$$\det[\partial_\tau + \mathcal{H}_e] = \prod_n \prod_{j,\boldsymbol{k}} (-i\omega_n + E_{j\boldsymbol{k}}), \tag{3.10}$$

where $\omega_n = (2n + 1)\pi/\beta$ is the Matsubara frequency for fermions.

From the grand potential, the mean-field (MF) values for m^A, m^B, M^A, and M^B are obtained as

$$m_{\mathrm{MF}}^A = \frac{1}{N} \frac{\partial \Omega_e}{\partial J^A M^A}, \tag{3.11}$$

$$m_{\mathrm{MF}}^B = \frac{1}{N} \frac{\partial \Omega_e}{\partial J^B M^B}, \tag{3.12}$$

$$M_{\mathrm{MF}}^A = \frac{1}{N} \frac{\partial \Omega_S}{\partial J^A m^A}, \tag{3.13}$$

$$M_{\mathrm{MF}}^B = \frac{1}{N} \frac{\partial \Omega_S}{\partial J^B m^B}. \tag{3.14}$$

They are also derived from $\frac{\partial \Omega}{\partial M^A} = \frac{\partial \Omega}{\partial M^B} = \frac{\partial \Omega}{\partial m^A} = \frac{\partial \Omega}{\partial m^B} = 0$. In terms of m_t, m_r, M_f, and M_5, the MF values are given as

$$m_{t,\mathrm{MF}} = \frac{1}{N} \frac{\partial \Omega_e}{\partial M_f}$$

$$= -\frac{1}{N} \sum_{\boldsymbol{k}} \left[\frac{M_f + \sqrt{d_s^2 + M_5^2}}{e_{1\boldsymbol{k}}} n_F(E_{1\boldsymbol{k}}) \right.$$

$$\left. + \frac{M_f - \sqrt{d_s^2 + M_5^2}}{e_{2\boldsymbol{k}}} n_F(E_{2\boldsymbol{k}}) \right], \tag{3.15}$$

$$m_{r,\mathrm{MF}} = \frac{1}{N} \frac{\partial \Omega_e}{\partial M_5}$$

$$= -\frac{1}{N} \sum_{\boldsymbol{k}} M_5 \left[\frac{1 + M_f/\sqrt{d_s^2 + M_5^2}}{e_{1\boldsymbol{k}}} n_F(E_{1\boldsymbol{k}}) \right.$$

$$\left. + \frac{1 - M_f/\sqrt{d_s^2 + M_5^2}}{e_{2\boldsymbol{k}}} n_F(E_{2\boldsymbol{k}}) \right], \tag{3.16}$$
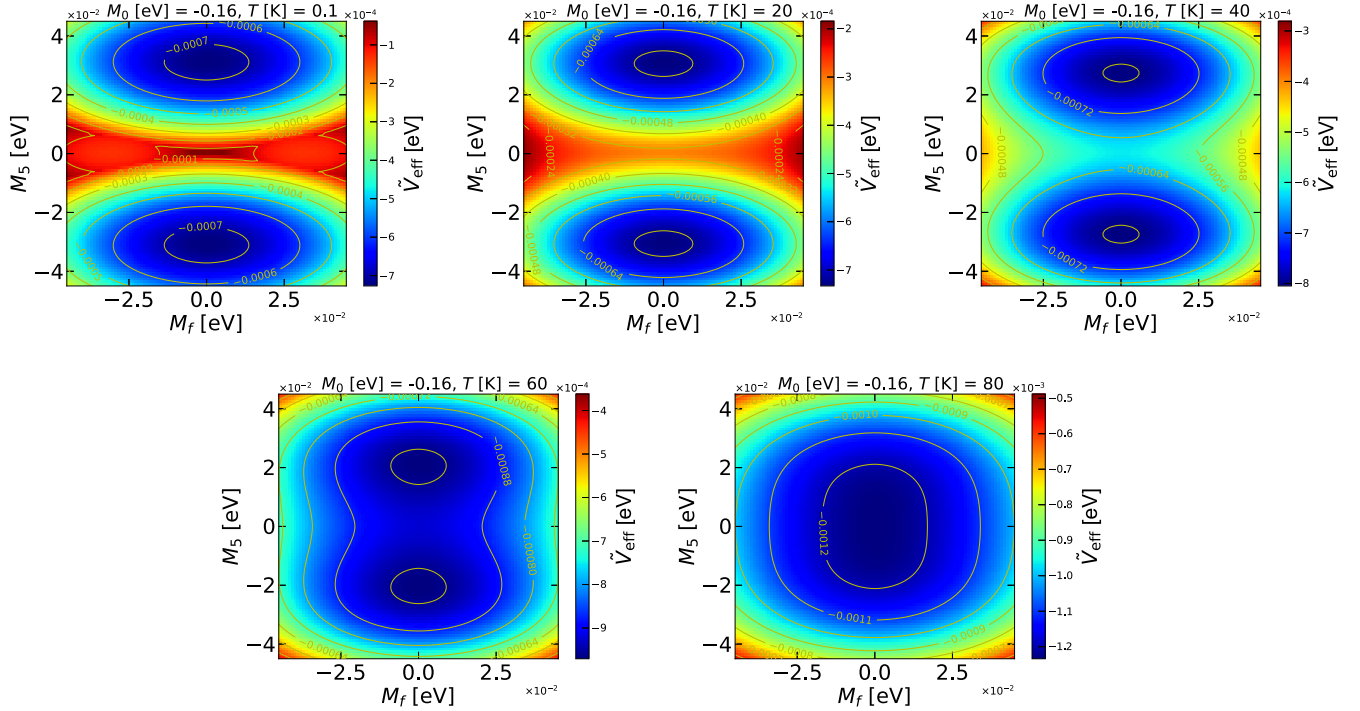
FIG. 1. Color map of the normalized effective potential $\tilde{V}_{\text{eff}} = [V_{\text{eff}}(M_f, M_5) - V_{\text{eff}}(0,0)]\ell^3$ on (M_f, M_5) plane. The parameters are $J^A = J^B = 0.25$ eV, $S = 5/2$, $x = 0.05$, $A_2 = 2A_1 = 0.4$ eV, $B_2 = 2B_1 = -0.4$ eV, and $M_0 = -0.16$ eV. The temperature is taken to be 0.1, 40, 60, and 80 K. At each panel, the contours of the potential are shown in solid yellow lines.

$$M_{f,\text{MF}} = -\frac{1}{2}xS[J^A B_S(S\beta J^A m^A) + J^B B_S(S\beta J^B m^B)], \quad (3.17)$$

$$M_{5,\text{MF}} = -\frac{1}{2}xS[J^A B_S(S\beta J^A m^A) - J^B B_S(S\beta J^B m^B)], \quad (3.18)$$

where $n_F(E) = 1/(1 + e^{\beta E})$ is the Fermi distribution function and B_S is the Brillouin function.

Since we are interested in the dynamics with respect to M_f and M_5 around possible stationary points, we put the MF values for the electron spins m_t and m_r and define the effective action for M_f and M_5 as[7]

$$\Omega|_{m_t=m_{t,\text{MF}},\, m_r=m_{r,\text{MF}}} \equiv -\beta^{-1} \ln e^{-\mathcal{S}_{\text{eff}}}. \quad (3.19)$$

Consequently the effective potential for M_f and M_5 is given by

$$V_{\text{eff}}(M_f, M_5) = \frac{1}{\beta V}\mathcal{S}_{\text{eff}} = \frac{1}{V}\Omega|_{m_t=m_{t,\text{MF}},\, m_r=m_{r,\text{MF}}}, \quad (3.20)$$

where V is the volume of the system. Here we omit the kinetic terms for the fluctuation around the stationary values for M_f and M_5. The derivation of the kinetic term is given in Appendix D. We will use the effective potential and the kinetic term to calculate the axion mass in Sec. V.

IV. MAGNETIC STATES

Let us see possible magnetic states, which are determined by the grand potential or equivalently the effective potential

---

[7]In Appendix B we give another aspect of the definition of the effective action.

given in Eq. (3.20). Figure 1 shows the effective potential on the (M_f, M_5) plane for various values of temperature. In the calculation we take the model parameters as those proposed by the first-principles calculation [1,24,27,30] and the values are given in the figure caption. In the figure we plot the effective potential normalized as $\tilde{V}_{\text{eff}} \equiv [V_{\text{eff}}(M_f, M_5) - V_{\text{eff}}(0,0)]\ell^3$. For $J^A = J^B > 0$ we find that the global minimum of the potential corresponds to $M_f = 0$ and nonzero $M_5 = M_{50}$. Here M_{50} is the stationary value for M_5. At the zero-temperature limit, $|M_{50}| = xSJ^A$ is expected from Eq. (3.18), which is consistent with the figure. It is also clear that the minimum is stable. This is also checked analytically, which is shown in Appendix C. At the minimum $m_A \simeq -m_B$ is realized, which means that the magnetic order of the electrons is the AFM. The same is true for M^A and M^B, i.e., $M^A \simeq -M^B$. The AFM disappears for temperature above the critical temperature T_c^{AFM}, which is around 80 K in the figure. In the region $T > T_c^{\text{AFM}}$, the global minimum is at the origin. Namely, all the MF values are zero and the insulator becomes the paramagnetic state.

The same result is obtained for $J^A = -J^B$, except that $M^A \simeq M^B$ is realized. In addition, we find that the effective potential does not drastically change depending on the sign of M_0, i.e., the topological phase or not. On the other hand, M_0 moderately affects the obseerevables, such as critical temperature and axion mass, which will be discussed below and in Sec. V.

Meanwhile the global minimum is the AFM state, we find that at low temperature there is a local minimum or a metastable point at $M_5 = 0$ and nonzero $M_f = M_{f0}$, which corresponds to the FM state. Here M_{f0} is the stationary value for M_f at a given temperature. To show this explicitly, we
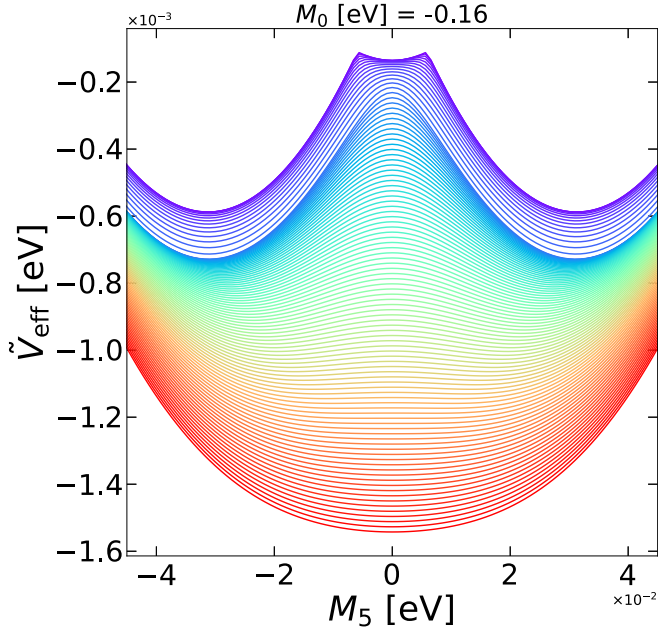
FIG. 2. Normalized effective potential $\tilde{V}_{\text{eff}} = [V_{\text{eff}}(M_f, M_5) - V_{\text{eff}}(0,0)]\ell^3$ with $M_f = M_{f0}$ as a function of M_5 for various values of temperature $T = 0.1$ to 100 K from top to bottom. The other parameters are the same as Fig. 1.

compute the effective potential as a function of M_5 by taking $M_f = M_{f0}$, which is given in Fig. 2. In the calculation the other parameters are the same as Fig. 1. The local minimum locates at $M_5 = 0$ at a sufficiently low temperature and it disappears for $T \gtrsim 10$ K. When the temperature gets even higher, the global minimum eventually reduces to $(M_f, M_5) = (0,0)$. We note that the result that the AFM state is the ground state while there is a metastable FM state is consistent with the first-principles calculation for $\text{Mn}_2\text{Bi}_2\text{Te}_5$ [21].

The result that the AFM state is lower than the FM one can be confirmed analytically as follows. The total energy is calculated from the free energy

$$E = \frac{\partial}{\partial \beta}\beta\Omega + \mu N n = E_e + E_S + E_R, \quad (4.1)$$

where $N n = -\partial\Omega/\partial\mu$ and

$$E_e = \sum_{j,\boldsymbol{k}}(E_{j\boldsymbol{k}} + \mu)n_F(E_{j\boldsymbol{k}}), \quad (4.2)$$

$$E_S = -N_s S[J^A m^A B_S(S\beta J^A m^A) + J^B m^B B_S(S\beta J^B m^B)]. \quad (4.3)$$

Taking the MF values for M^A and M^B at the zero-temperature limit, it is simply given by

$$E = E_e = -\sum_{\boldsymbol{k}}(e_{1\boldsymbol{k}} + e_{2\boldsymbol{k}}). \quad (4.4)$$

From Eqs. (2.22) and (2.23), it is straightforward to check that $E|_{M_f=0,M_5=\bar{M}} - E|_{M_f=\bar{M},M_5=0} < 0$ for any values of $\bar{M}$ and $\boldsymbol{k}$. This is why the AFM is the lowest-energy state. See also Appendix C for the discussion of the FM order for each sublattice.

To get the whole picture, we plot the phase diagram regarding the magnetic order on (M_0, T) plane in Fig. 3. The shaded
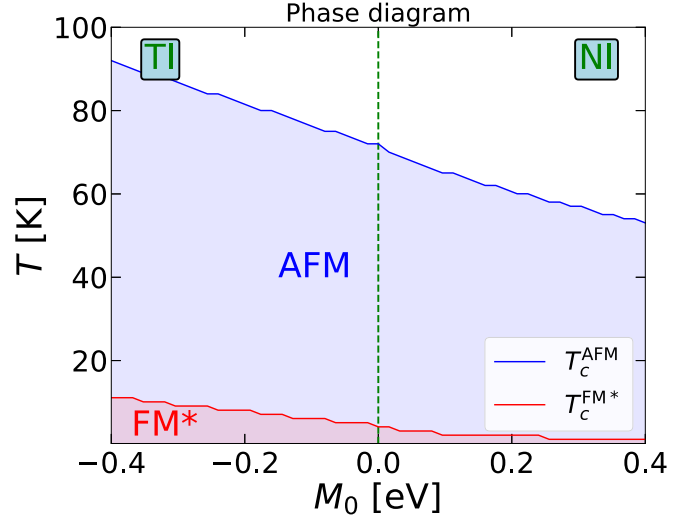

FIG. 3. Phase diagram of the magnetic state. The AFM state and metastable FM state are indicated as "AFM" and "FM∗," respectively. Here J^A, J^B, S, x, A_i, and B_i ($i = 1, 2$) are taken as the same as Fig. 1. T_c^{AFM} is the critical temperature of the AFM state and the region $T < T_c^{\text{AFM}}$ the AFM state becomes the global minimum. $T_c^{\text{FM∗}}$ is the critical temperature between the metastable FM state and the AFM state. As a reference, we indicate the topological and normal phases of insulator as "TI" and "NI," respectively, which is separated by a vertical line $M_0 = 0$ (green dashed).

region shows the AFM or FM states. In the low temperature below $\mathcal{O}(10^2 \text{ K})$, the magnetic state is the AFM. On the other hand, at sufficiently low temperature that is less than $\mathcal{O}(10 \text{ K})$, the metastable FM state appears. Here we denote $T_c^{\text{FM∗}}$ as the critical temperature. We note that the stable AFM state also exists at the temperature, which indicates a possible phase transition between the metastable FM state and the AFM state. While the critical temperatures T_c^{AFM} and $T_c^{\text{FM∗}}$ depend on the value of M_0, the sign of M_0, i.e., the topological phase or not, does not have a significant impact on them. In the next section, we compute the mass of the dynamical axion for the AFM and the FM states.

V. AXION MASS

As discussed in Ref. [15], the dynamical axion field is defined as the quantum fluctuation around the minimum of the potential in M_5 direction. As shown in the previous section there are two possible minima; the AFM and metastable FM states. Expanding M_5 as $M_5 \equiv M_{50} + \varphi$ around the minima, the axion field a is defined as

$$V_{\text{eff}} = V_{\text{eff}}(M_{f0}, M_{50})$$
$$+ \frac{1}{2}g^2 \frac{\partial^2 V_{\text{eff}}}{\partial M_5^2}\bigg|_{M_f=M_{f0}, M_5=M_{50}} a^2 + \mathcal{O}(a^4). \quad (5.1)$$

Here $g = \frac{d\Phi}{d\theta}|_{\theta=\theta_0}$ where $\Phi(\theta) = M_5$ is the inverse function of θ defined by [1]

$$\theta(M_5) = \frac{1}{4\pi}\int d^3k \frac{2|d| + d^4}{(|d| + d^4)^2 |d|^3}\epsilon^{ijkl}d^i\partial_{k_x}d^j\partial_{k_y}d^k\partial_{k_z}d^l. \quad (5.2)$$
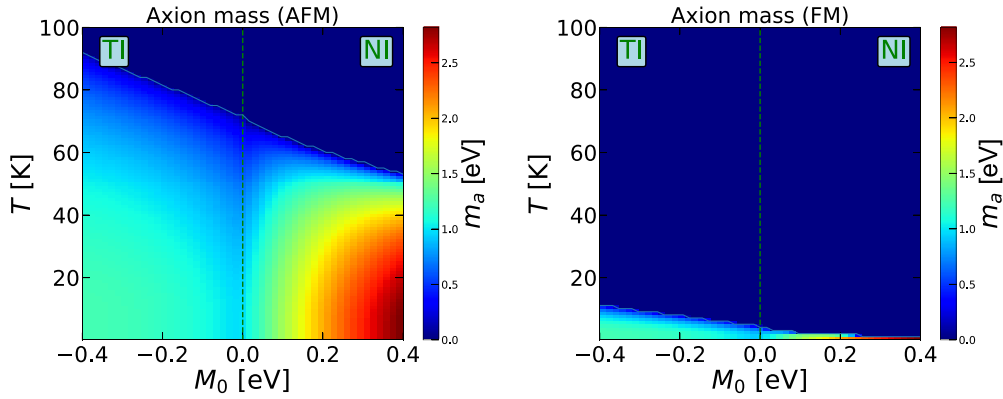
FIG. 4. Color map of the axion mass under the AFM state (left) and the metastable FM state (right). Here J^A, J^B, S, x, A_i, and B_i ($i = 1, 2$) are taken as the same as Fig. 1. As in Fig. 3, topological and normal phases are indicated as "TI" and "NI," respectively.

In the expression we define $|d|^2$ as $|d|^2 \equiv \sum_{a=1}^5 d^a d^a$ where $d^5 = M_5$ and ϵ^{ijkl} is the Levi-Civita symbol with i, j, k, l being 1, 2, 3, and 5. A parameter θ_0 satisfies $\Phi(\theta_0) = M_{50}$. Then the mass m_a of the dynamical axion is given by

$$K_a m_a^2 = \frac{1}{2V} \frac{\partial^2 V_{\text{eff}}}{\partial M_5^2}\bigg|_{M_f=M_{f0}, M_5=M_{50}}, \quad (5.3)$$

where K_a is the stiffness. For reference, see Appendix C for the analytic expression of the second derivative of V_{eff} in the zero-temperature limit. In the Appendix we check that Eqs. (C1) and (C2), which are the second derivatives with respect to M_f and M_5, respectively, correspond to the spin susceptibility calculated in the linear perturbation theory. The stiffness is given by the perturbative expansion with respect to φ. Details are given in Appendix D and the result is

$$K_a = \frac{1}{V} \sum_{\mathbf{k}} \frac{d_0^2}{4(d_0^2 + M_{50}^2)^{5/2}}, \quad (5.4)$$

for the AFM states and

$$K_a = \frac{1}{V} \sum_{\mathbf{k}} \frac{(d_0^2 - d_s^2 + M_{f0}^2)(e_{2k} - e_{1k}) + ds M_{f0}(e_{1k} + e_{2k})}{8ds^3 M_{f0} e_{1k} e_{2k}}, \quad (5.5)$$

for the FM states. It is clear that the functions in the summation are positive, irrespective of the wave number. From Eqs. (5.3), (5.4), and (5.5), we evaluate the axion mass.

As shown in the previous section, there are two possible magnetic states, the AFM state and metastable FM state. Thus we evaluate the axion mass for both states. Figure 4 shows the axion mass on the (M_0, T) plane for the AFM state and the metastable FM state. We find that the axion mass is $\mathcal{O}(\text{eV})$ for both states, except for the phase boundaries. This result is consistent with Ref. [15] where only the AFM state is considered at zero temperature in the Hubbard model. Here we see a mild dependence of the mass on the sign of M_0. At the phase boundaries, the axion mass approaches zero from the AFM state to the paramagnetic state or from the metastable FM state to the AFM state. Therefore the axion mass can be, in principle, various values by optimizing the temperature. This result is quantitatively consistent with Ref. [29], meanwhile the typical value of the axion mass is different. The typical

energy scale of the mass is eV, which is the same as one estimated in the Hubbard model [15]. On the other hand, the mass scale is not reduced by the value of the energy gap, which is a different feature from the results in the Hubbard model. The result has a direct impact on the projected mass range of the *particle* axion in the proposal [3]. Namely, the targeted mass range is typically eV, not meV. If the insulator near the phase boundary is realized, a more suppressed mass range could be probed. However, preparation of such a state of insulators may not be trivial and there would be technical challenges for the realistic observation.

It is worth noting that there are two types of axion for the AFM and FM states. They could be utilized in future *particle* axion search. For example, we speculate that in the circumstance of the FM state, the *particle* axion induces an excitation of the dynamical axion and it may cause the phase transition to the AFM state, which can be a possible signal of axion detection. As we mentioned, the axion mass is not severely influenced by the topology of the insulators. This is true for both the AFM and the metastable FM states. Therefore, various insulators that are not in the topological phase are also possible candidates of material for the search of the *particle* axion and axion-like particles. We hope this remark will inspire future studies for finding realistic materials for *particle* axion detection experiments.

VI. CONCLUSION

In this study we formulated the mass of the dynamical axion in the magnetically doped topological insulators. To this end, we considered the 3D effective model of TIs with the interaction terms between the electrons and the impurities. We found that the antiferromagnetic state is the ground state at low temperature. Besides, the ferromagnetic state appears as a metastable state under sufficiently low temperature. In both magnetic states, the axion mass is found to be $\mathcal{O}(\text{eV})$ and it goes to zero as the temperature approaches the critical temperature, i.e., the phase boundary. We checked the results by computing the Van Vleck-type spin susceptibility for a band in linear response theory. In addition, we found a strong independence of the energy gap on the axion mass scale. Therefore, the typical mass scale of the *particle* axion search proposed in Ref. [3] should be eV.

The fact that the axion mass can be controlled by temperature may be suitable for the detection of the *particle* axion. Specifically, the phase boundary has a potential to search the *particle* axion with a suppressed mass. In addition, there can be various magnetic states indicated in first-principles calculation, for example, in $Mn_2Bi_2Te_5$ [21]. To describe such rich magnetic states rather than the AFM or FM, we need a further extension of the model, which would be another interesting area of research to find out the mass of the dynamical axion in a more complicated phase diagram. We leave it for future work.

APPENDIX A: GAMMA MATRICES

The Gamma matrices Γ^a ($a = 1, \ldots, 4$) in Eq. (2.2) are defined as

$$\Gamma^1 = \begin{pmatrix} 0 & \sigma^1 \\ \sigma^1 & 0 \end{pmatrix}, \quad \Gamma^2 = \begin{pmatrix} 0 & \sigma^2 \\ \sigma^2 & 0 \end{pmatrix},$$

$$\Gamma^3 = \begin{pmatrix} 0 & -i \\ i & 0 \end{pmatrix}, \quad \Gamma^4 = \begin{pmatrix} 1 & 0 \\ 0 & -1 \end{pmatrix}. \quad (A1)$$

Γ^5 is defined by $\Gamma^5 = -\Gamma^1\Gamma^2\Gamma^3\Gamma^4$. In addition, we define $\Gamma^{ab} = [\Gamma^a, \Gamma^b]/(2i)$. To be explicit, they are given by

$$\Gamma^5 = \begin{pmatrix} 0 & \sigma^3 \\ \sigma^3 & 0 \end{pmatrix}, \quad \Gamma^{12} = \begin{pmatrix} \sigma^3 & 0 \\ 0 & \sigma^3 \end{pmatrix}. \quad (A2)$$

In the sublattice basis, the Gamma matrices are given by

$$\Gamma^{1\prime} = \begin{pmatrix} \sigma^1 & 0 \\ 0 & -\sigma^1 \end{pmatrix}, \quad \Gamma^{2\prime} = \begin{pmatrix} \sigma^2 & 0 \\ 0 & -\sigma^2 \end{pmatrix},$$

$$\Gamma^{3\prime} = \begin{pmatrix} 0 & -i \\ i & 0 \end{pmatrix}, \quad \Gamma^{4\prime} = \begin{pmatrix} 0 & -1 \\ -1 & 0 \end{pmatrix}, \quad (A3)$$

$$\Gamma^{5\prime} = \begin{pmatrix} \sigma^3 & 0 \\ 0 & -\sigma^3 \end{pmatrix}, \quad \Gamma^{12\prime} = \begin{pmatrix} \sigma^3 & 0 \\ 0 & \sigma^3 \end{pmatrix}. \quad (A4)$$

APPENDIX B: EFFECTIVE ACTION

Since we consider the half-filling case, i.e., the number of electrons is fixed, the grand potential $\Omega_e(M^A, M^B)$ of the electron part corresponds to the Helmholtz free energy $F_e(M^A, M^B)$. The Gibbs free energy $G_e(m^A, m^B)$ is then given by the Legendre transformation

$$G_e(m^A, m^B) = -\sum_{I=A,B} \frac{\partial F_e}{\partial M^I} M^I + F_e$$

$$= -N \sum_{I=A,B} J^I m^I M^I + F_e, \quad (B1)$$

where $m^I \equiv (1/N)\partial F_e/\partial(J^I M^I)$ ($I = A, B$). This definition is equivalent to the MF values for m^A and m^B given in Eqs. (3.11)

and (3.12). In addition, $G_e(m^A, m^B)$ is equivalent to $\Omega_e + H_R$ where m^I are taken to be their the MF values. Since the Gibbs free energy corresponds to the effective action in the quantum field theory, Eq. (3.19) is considered as the effective action. In our analysis we give Eq. (3.19) as a function of M_f and M_5, i.e., $m^I = m^I(M^I)$, instead of m^I itself since we are interested in the dynamical field around the minimum (M_{f0}, M_{50}).

APPENDIX C: MASS AT ZERO TEMPERATURE AND SPIN SUSCEPTIBILITY

At the zero temperature, $\Omega_S + H_R$ in Ω cancels. Then the curvature around the minimum is computed easily. The results are

$$\frac{1}{2}\frac{\partial^2\Omega}{\partial M_f^2}\bigg|_{M_f=M_{f0},M_5=M_{50}}$$

$$= \frac{1}{2}\frac{\partial^2\Omega_e}{\partial M_f^2}\bigg|_{M_f=M_{f0},M_5=M_{50}}$$

$$= \frac{1}{2}\sum_k (d_0^2 - d_s^2)\left[\frac{1}{e_{1k}^3} + \frac{1}{e_{2k}^3}\right]_{M_f=M_{f0},M_5=M_{50}}, \quad (C1)$$

$$\frac{1}{2}\frac{\partial^2\Omega}{\partial M_5^2}\bigg|_{M_f=M_{f0},M_5=M_{50}}$$

$$= \frac{1}{2}\frac{\partial^2\Omega_e}{\partial M_5^2}\bigg|_{M_f=M_{f0},M_5=M_{50}}$$

$$= \frac{1}{2}\sum_k\left[-M_5^2\left\{\frac{\left(1 + \frac{M_f}{\sqrt{d_s^2+M_5^2}}\right)^2}{e_{1k}^3} + \frac{\left(1 - \frac{M_f}{\sqrt{d_s^2+M_5^2}}\right)^2}{e_{2k}^3}\right\}\right.$$

$$\left. + \frac{1 + \frac{M_f d_s^2}{(d_s^2+M_5^2)^{3/2}}}{e_{1k}} + \frac{1 - \frac{M_f d_s^2}{(d_s^2+M_5^2)^{3/2}}}{e_{2k}}\right]_{M_f=M_{f0},M_5=M_{50}}. \quad (C2)$$

It is clear that both quantities are positive and we checked that $\partial^2\Omega/\partial M_f\partial M_5 = 0$ at the minimum. Therefore, the minimum is stable.

The above results can be confirmed by the spin susceptibility of electron computed in linear response theory. In the magnetic TIs, the local spins have an effective interaction via electrons. In the present case it corresponds to $-\tilde{J}_f^{\mathrm{eff}} M_f M_f$ and $-\tilde{J}_5^{\mathrm{eff}} M_5 M_5$, where the normalized effective exchange couplings are given by $\tilde{J}_f^{\mathrm{eff}} = \chi_f^e/2$ and $\tilde{J}_5^{\mathrm{eff}} = \chi_5^e/2$ [31].[8] Here χ_f^e and χ_5^e are the Van Vleck-type spin susceptibility for a band insulator. Namely, χ_f^e and χ_5^e correspond to the squared mass parameters. By taking $\mathcal{H}_k^m$ as the perturbation in liner response theory they are calculated

---

[8]A factor of 2 is different compared to the expression given in Ref. [31]. We start with the Hamiltonian $1/(2\chi_f^e)m_t^2 + 1/(2\chi_5^e)m_r^2 - (M_f m_t + M_5 m_r)$ to obtain $-(1/2)\chi_f^e M_f M_f - (1/2)\chi_5^e M_5 M_5$.

as

$$\chi_f^e = \sum_{\boldsymbol{k},m,n} [n_F(E_{n\boldsymbol{k}}) - n_F(E_{m\boldsymbol{k}})] \frac{\langle u_{n\boldsymbol{k}}|\Gamma^{12}|u_{m\boldsymbol{k}}\rangle \langle u_{m\boldsymbol{k}}|\Gamma^{12}|u_{n\boldsymbol{k}}\rangle}{E_{m\boldsymbol{k}} - E_{n\boldsymbol{k}}}, \quad (C3)$$

$$\chi_5^e = \sum_{\boldsymbol{k},m,n} [n_F(E_{n\boldsymbol{k}}) - n_F(E_{m\boldsymbol{k}})] \frac{\langle u_{n\boldsymbol{k}}|\Gamma^5|u_{m\boldsymbol{k}}\rangle \langle u_{m\boldsymbol{k}}|\Gamma^5|u_{n\boldsymbol{k}}\rangle}{E_{m\boldsymbol{k}} - E_{n\boldsymbol{k}}}, \quad (C4)$$

where $E_{n\boldsymbol{k}}$ and $|u_{n\boldsymbol{k}}\rangle$ are the energy eigenvalues and eigenstates of the electron, respectively, which is obtained by diagonalizing $\mathcal{H}_{\boldsymbol{k}}^{\text{TI}}$.

To compare the spin susceptibilities given in Eqs. (C3) and (C4), it is appropriate to start with the free energy $\Omega' \equiv \Omega_e - N(M_f m_t + M_5 m_r)$, where the free energy for the local spin is omitted. This is because the spin susceptibilities given above are obtained in the linear response theory by taking the $-(M_f m_t + M_5 m_r)$ term as the perturbation while H_e is the zeroth-order Hamiltonian. Then it is straightforward to get

$$\frac{1}{2}\frac{\partial^2 \Omega'}{\partial M_f^2}\bigg|_{M_f=M_{f0},M_5=M_{50}} = -\frac{1}{2}\frac{\partial^2 \Omega_e}{\partial M_f^2}\bigg|_{M_f=M_{f0},M_5=M_{50}}, \quad (C5)$$

$$\frac{1}{2}\frac{\partial^2 \Omega'}{\partial M_5^2}\bigg|_{M_f=M_{f0},M_5=M_{50}} = -\frac{1}{2}\frac{\partial^2 \Omega_e}{\partial M_5^2}\bigg|_{M_f=M_{f0},M_5=M_{50}}. \quad (C6)$$

In fact, we confirmed that

$$\frac{1}{2}\frac{\partial^2 \Omega_e}{\partial M_f^2}\bigg|_{M_f=0,M_5=0} = \frac{1}{2}\chi_f^e = \sum_{\boldsymbol{k}} \frac{1 - d_s^2/d_0^2}{d_0}, \quad (C7)$$

$$\frac{1}{2}\frac{\partial^2 \Omega_e}{\partial M_5^2}\bigg|_{M_f=0,M_5=0} = \frac{1}{2}\chi_5^e = \sum_{\boldsymbol{k}} \frac{1}{d_0}. \quad (C8)$$

Moreover, since Eqs. (C3) and (C4) from the linear response theory can be applied for a generic form of the Hamiltonian, it would be possible to take $\mathcal{H}_{e\boldsymbol{k}}|_{M_f=M_{f0},M_5=M_{50}}$ and $\delta M_f \Gamma^{12} + \delta M_5 \Gamma^5$ as the primary Hamiltonian and perturbation, respectively. See also Appendix D for such an expansion. In that case, $E_{n\boldsymbol{k}}$ and $|u_{n\boldsymbol{k}}\rangle$ correspond to the energy eigenvalues and eigenstates of the Hamiltonian $\mathcal{H}_{e\boldsymbol{k}}$ where $M_f = M_{f0}$ and $M_5 = M_{50}$. By computing χ_f^e and χ_5^e numerically, we checked the correspondence between the mass squared and the Van Vleck-type spin susceptibility

$$\frac{1}{2}\frac{\partial^2 \Omega_e}{\partial M_f^2}\bigg|_{M_f=M_{f0},M_5=M_{50}} = \frac{1}{2}\chi_f^e, \quad (C9)$$

$$\frac{1}{2}\frac{\partial^2 \Omega_e}{\partial M_5^2}\bigg|_{M_f=M_{f0},M_5=M_{50}} = \frac{1}{2}\chi_5^e, \quad (C10)$$

for any value of M_{f0} and M_{50}.

Additionally, we checked that the spin susceptibilities for the sublattice A and B, which are defined by

$$\chi_A^e = \sum_{\boldsymbol{k},m,n} [n_F(E_{n\boldsymbol{k}}) - n_F(E_{m\boldsymbol{k}})] \frac{\langle u_{n\boldsymbol{k}}|(\Gamma^{12}+\Gamma^5)/2|u_{m\boldsymbol{k}}\rangle \langle u_{m\boldsymbol{k}}|(\Gamma^{12}+\Gamma^5)/2|u_{n\boldsymbol{k}}\rangle}{E_{m\boldsymbol{k}} - E_{n\boldsymbol{k}}}, \quad (C11)$$

$$\chi_B^e = \sum_{\boldsymbol{k},m,n} [n_F(E_{n\boldsymbol{k}}) - n_F(E_{m\boldsymbol{k}})] \frac{\langle u_{n\boldsymbol{k}}|(\Gamma^{12}-\Gamma^5)/2|u_{m\boldsymbol{k}}\rangle \langle u_{m\boldsymbol{k}}|(\Gamma^{12}-\Gamma^5)/2|u_{n\boldsymbol{k}}\rangle}{E_{m\boldsymbol{k}} - E_{n\boldsymbol{k}}}, \quad (C12)$$

are both positive. This result is also expected since the order of each sublattice is the FM.

APPENDIX D: PROPAGATOR AND THE STIFFNESS

The stiffness is given by the coefficient of the axion kinetic term.[9] To give the kinetic term we consider a fluctuation of M_5 around the stationary point by promoting M_5 as a dynamical degree of freedom. To make the discussion generic, we take $M_5 = M_{50} + \varphi$. The kinetic term is obtained by expanding $\mathcal{S}_e$ with respect to φ. To this end, we write $\mathcal{H}_e = \mathcal{H} + \delta\mathcal{H}$. In the wave-number space, they are defined as

$$\mathcal{H}_{\boldsymbol{k}} = \mathcal{H}_{\boldsymbol{k}}^{\text{TI}} + M_{f0}\Gamma^{12} + M_{50}\Gamma^5, \quad (D1)$$

$$\delta\mathcal{H}_{\boldsymbol{k}} = \varphi\Gamma^5. \quad (D2)$$

Using $\ln\det[\partial_\tau + \mathcal{H}_e] = \operatorname{Tr}\ln[\partial_\tau + \mathcal{H}_e]$ and

$$\operatorname{Tr}\ln(\partial_\tau + \mathcal{H} + \delta\mathcal{H}) = \operatorname{Tr}\ln(-G^{-1}) - \sum_{n=1}^{\infty} \operatorname{Tr}(G\delta\mathcal{H})^n, \quad (D3)$$

where $G^{-1} = -\partial_\tau - \mathcal{H}$, the kinetic term is obtained from the quadratic term in the second term of Eq. (D3):

$$\operatorname{Tr}(G\delta\mathcal{H})^2 = \frac{V^2}{N^2}\int_0^\beta d\tau_i \int_0^\beta d\tau_j$$
$$\times \sum_{x_i,x_j} \operatorname{Tr}[G(x_i - x_j)\delta\mathcal{H}(x_j)G(x_j - x_i)\delta\mathcal{H}(x_i)]. \quad (D4)$$

Here the arguments of G and $\delta\mathcal{H}$ represent $x_i = (\tau_i, \boldsymbol{x}_i)$. The propagator and the field $\delta\mathcal{H}$ are expanded as

$$G(x_i - x_j) = \frac{1}{\beta V}\sum_{i\omega_n}\sum_{\boldsymbol{k}} \tilde{G}(k)e^{-i\omega_n(\tau_1-\tau_2)+i\boldsymbol{k}\cdot(\boldsymbol{x}_i-\boldsymbol{x}_j)}, \quad (D5)$$

$$\delta\mathcal{H}(x_i) = \frac{1}{\beta V}\sum_{i\omega_n}\sum_{\boldsymbol{k}} \delta\tilde{\mathcal{H}}(k)e^{-i\omega_n\tau+i\boldsymbol{k}\cdot\boldsymbol{x}_i}, \quad (D6)$$

---

[9]The authors of Ref. [32] gave a similar calculation using the Hubbard-Stratonovich transformation, but to discuss topological superconductors and superfluids. See also Ref. [33] for the renormalization group approach.

where $\tilde{G}^{-1}(k) = i\omega_n - \mathcal{H}_{\boldsymbol{k}}$. Similarly to x_i, we take the argument k_i of $\tilde{G}$ and $\delta\tilde{\mathcal{H}}$ as $k_i = (i\omega_{ni}, \boldsymbol{k}_i)$. Then

$$\text{Tr}(G\delta\mathcal{H})^2$$

$$= \frac{1}{\beta^2 V^2} \sum_{i\omega_{n1}} \sum_{i\omega_{n2}} \sum_{\boldsymbol{k}_1, \boldsymbol{k}_2} \text{Tr}[\tilde{G}(k_1)\delta\tilde{\mathcal{H}}(k_2)\tilde{G}(k_1 - k_2)\delta\tilde{\mathcal{H}}(-k_2)].$$
(D7)

We find the propagator $\tilde{G}$ in the momentum space is given by

$$\tilde{G}(i\omega_n, \boldsymbol{q}) = \frac{1}{F}\left[(i\omega_n - \epsilon)g_0 + \sum_{a=1}^{5} g_1^a \Gamma^a + \sum_{a=1}^{4} g_2^a \Gamma^a \Gamma^5 \right.$$

$$\left. + \sum_{ab} g^{ab} \Gamma^{ab}\right],$$
(D8)

where $\epsilon = \epsilon_0 - \mu$ and

$$g_0 = (i\omega_n - \epsilon)^2 - d_0^2 - M_{50}^2 - M_{f0}^2,$$
(D9)

$$g_1^a = -d^a\{-(i\omega_n - \epsilon)^2 + d_0^2 + M_{50}^2 + M_{f0}^2\} \quad (a = 1, 2),$$
(D10)

$$g_1^a = -d^a\{-(i\omega_n - \epsilon)^2 + d_0^2 + M_{50}^2 - M_{f0}^2\} \quad (a = 3, 4, 5),$$
(D11)

$$g_2^1 = 2id^2 M_{50} M_{f0},$$
(D12)

$$g_2^2 = -2id^1 M_{50} M_{f0},$$
(D13)

$$g_2^3 = 2i(i\omega_n - \epsilon)d^4 M_{f0},$$
(D14)

$$g_2^4 = -2i(i\omega_n - \epsilon)d^3 M_{f0},$$
(D15)

$$g^{12} = \left\{(i\omega_n - \epsilon)^2 - (d^1)^2 - (d^2)^2 + (d^3)^2 + (d^4)^2\right.$$

$$\left. + M_{50}^2 - M_{f0}^2\right\}M_{f0},$$
(D16)

$$g^{34} = 2(i\omega_n - \epsilon)M_{50} M_{f0},$$
(D17)

$$g^{23} = 2d^1 d^3 M_{f0},$$
(D18)

$$g^{13} = -2d^2 d^3 M_{f0},$$
(D19)

$$g^{14} = -2d^2 d^4 M_{f0},$$
(D20)

$$g^{24} = 2d^1 d^4 M_{f0},$$
(D21)

$$F = \{(i\omega_n - \epsilon)^2 - |d_0|^2 - (M_{f0} - M_{50})^2\}\{(i\omega_n - \epsilon)^2$$

$$- |d_0|^2 - (M_{f0} + M_{50})^2\} - 4d_s^2 M_{f0}^2.$$
(D22)

Using the propagator, the stiffness is given by

$$K_a = -\frac{1}{2\beta V}\frac{\partial^2}{\partial(i\omega_{nk})^2}$$

$$\times \sum_{i\omega_{nq}, \boldsymbol{q}} \text{Tr}[\tilde{G}(i\omega_{nq}, \boldsymbol{q})\Gamma^5 \tilde{G}(i\omega_{nq} + i\omega_{nk}, \boldsymbol{q})\Gamma^5]\Bigg|_{i\omega_{nk}=0}.$$
(D23)

Here we redefined k_1 and k_2 as $k_1 = q$ and $k_2 = -k$ and taken $\boldsymbol{k} = 0$ in $\tilde{G}(q + k)$. This expression can be checked by taking $M_{f0} = 0$ to get

$$K_a = \frac{1}{V}\sum_{\boldsymbol{q}} \frac{d_0^2}{4(|d_0|^2 + M_{50}^2)^{5/2}},$$
(D24)

in the zero temperature limit, which agrees with the one given in Ref. [15]. This is the expression of the stiffness for the AFM state. The FM state corresponds to nonzero M_{f0} and $M_{50} = 0$. In that case, we find in the zero-temperature limit

$$K_a = \frac{1}{V}\sum_{\boldsymbol{q}} \frac{(d_0^2 - d_s^2 + M_{f0}^2)(e_{2\boldsymbol{q}} - e_{1\boldsymbol{q}}) + d_s M_{f0}(e_{1\boldsymbol{q}} + e_{2\boldsymbol{q}})}{8 d_s^3 M_{f0} e_{1\boldsymbol{q}} e_{2\boldsymbol{q}}},$$
(D25)

where $M_5 = 0$ is taken in $e_{1\boldsymbol{q}}$ and $e_{2\boldsymbol{q}}$. We note that the zero-temperature limit is a good approximation since we discuss the system at up to $\mathcal{O}(10^2)$ K, which is smaller than the typical energy scale of the electron energy.

The formalism given in the discrete space can be written in the continuum case by the following replacements:

$$\frac{1}{N}\sum_i \rightarrow \frac{1}{V}\int d^3x, \quad \frac{1}{V}\sum_{\boldsymbol{k}} \rightarrow \int \frac{d^3k}{(2\pi)^3},$$
(D26)

$$\sqrt{N}c_i \rightarrow \sqrt{V}\psi(\boldsymbol{x}), \quad Nn_i \rightarrow Vn(\boldsymbol{x}).$$
(D27)

Here ψ is the wave function of the electrons in the continuum space, $n = \psi^\dagger\psi$, and $n_i = c_i^\dagger c_i$.

[1] R. Li, J. Wang, X. Qi, and S. C. Zhang, Nat. Phys. **6**, 284 (2010).

[2] H. Ooguri and M. Oshikawa, Phys. Rev. Lett. **108**, 161803 (2012).

[3] D. J. E. Marsh, K. C. Fong, E. W. Lentz, L. Smejkal, and M. N. Ali, Phys. Rev. Lett. **123**, 121601 (2019).

[4] S. Chigusa, T. Moroi, and K. Nakayama, Phys. Rev. D **101**, 096013 (2020).

[5] S. Chigusa, T. Moroi, and K. Nakayama, J. High Energy Phys. 08 (2021) 074.

[6] X. L. Qi, T. L. Hughes, and S. C. Zhang, Phys. Rev. B **78**, 195424 (2008).

[7] X. L. Qi, R. Li, J. Zang, and S. C. Zhang, Science **323**, 1184 (2009).

[8] F. W. Hehl, Y. N. Obukhov, J. P. Rivera, and H. Schmid, Phys. Rev. A **77**, 022106 (2008).

[9] I. E. Dzyaloshinskii, Sov. Phys. JETP **10**, 628 (1959); D. N. Astrov, *ibid.* **11**, 708 (1960); **13**, 729 (1961).

[10] A. M. Essin, J. E. Moore, and D. Vanderbilt, Phys. Rev. Lett. **102**, 146805 (2009).

[11] L. Wu, M. Salehi, N. Koirala, J. Moon, S. Oh, and N. P. Armitage, Science **354**, 1124 (2016).

[12] A. Sekine and K. Nomura, J. Phys. Soc. Jpn. **83**, 104709 (2014).

[13] A. Sekine and K. Nomura, Phys. Rev. Lett. **116**, 096401 (2016).

[14] J. Schütte-Engel, D. J. E. Marsh, A. J. Millar, A. Sekine, F. Chadha-Day, S. Hoof, M. N. Ali, K. C. Fong, E. Hardy, and L. Šmejkal, J. Cosmol. Astropart. Phys. **2021**, 066 (2021).

[15] K. Ishiwata, Phys. Rev. D **104**, 016004 (2021).

[16] J. Li, C. Wang, Z. Zhang, B. L. Gu, W. Duan, and Y. Xu, Phys. Rev. B **100**, 121103(R) (2019).

[17] H. Li, S. Y. Gao, S. F. Duan, Y. F. Xu, K. J. Zhu, S. J. Tian, J. C. Gao, W. H. Fan, Z. C. Rao, J. R. Huang *et al.*, Phys. Rev. X **9**, 041039 (2019).

[18] J. Li *et al.*, Sci. Adv. **5**, eaaw5685 (2019).

[19] D. Zhang, M. Shi, T. Zhu, D. Xing, H. Zhang, and J. Wang, Phys. Rev. Lett. **122**, 206401 (2019).

[20] Y. J. Hao, P. Liu, Y. Feng, X. M. Ma, E. F. Schwier, M. Arita, S. Kumar, C. Hu, R. Lu, M. Zeng *et al.*, Phys. Rev. X **9**, 041038 (2019).

[21] Y. Li, Y. Jiang, J. Zhang, Z. Liu, Z. Yang, and J. Wang, Phys. Rev. B **102**, 121107(R) (2020).

[22] J. Zhang, D. Wang, M. Shi, T. Zhu, H. Zhang, and J. Wang, Chin. Phys. Lett. **37**, 077304 (2020).

[23] L. Cao, S. Han, Y. Y. Lv, D. Wang, Y. C. Luo, Y. Y. Zhang, S. H. Yao, J. Zhou, Y. B. Chen, H. Zhang, and Y. F. Chen, Phys. Rev. B **104**, 054421 (2021).

[24] H. Zhang, C. X. Liu, X. L. Qi, X. Dai, Z. Fang, and S. C. Zhang, Nat. Phys. **5**, 438 (2009).

[25] C. X. Liu, X. L. Qi, H. J. Zhang, X. Dai, Z. Fang, and S. C. Zhang, Phys. Rev. B **82**, 045122 (2010).

[26] R. Yu, W. Zhang, H. J. Zhang, S. C. Zhang, X. Dai, and Z. Fang, Science **329**, 61 (2010).

[27] G. Rosenberg and M. Franz, Phys. Rev. B **85**, 195119 (2012).

[28] D. Kurebayashi and K. Nomura, J. Phys. Soc. Jpn. **83**, 063709 (2014).

[29] J. Wang, B. Lian, and S. C. Zhang, Phys. Rev. B **93**, 045115 (2016).

[30] L. Fu and E. Berg, Phys. Rev. Lett. **105**, 097001 (2010).

[31] J. Wang, B. Lian, and S. C. Zhang, Phys. Rev. Lett. **115**, 036805 (2015).

[32] K. Shiozaki and S. Fujimoto, Phys. Rev. B **89**, 054506 (2014).

[33] B. Roy, P. Goswami, and J. D. Sau, Phys. Rev. B **94**, 041101(R) (2016).